NMR Transversal Relaxivity of Suspensions of Lanthanide Oxide Nanoparticles

Małgorzata Norek,[†] Giovannia A. Pereira,[‡] Carlos F. G. C. Geraldes,[‡] Antonia Denkova,[§] Wuzong Zhou,[#] and Joop A. Peters*[,†]

Biocatalysis and Organic Chemistry, Department of Biotechnology, Delft University of Technology, Julianalaan 136, 2628 BL Delft, The Netherlands, NMR Center and Center of Neuroscience and Cell Biology, Department of Biochemistry, University of Coimbra, P. O. Box 3126, 3001-401 Coimbra, Portugal, Physical Chemistry and Molecular Thermodynamics, Delft University of Technology, 2628 BL Delft, The Netherlands, and School of Chemistry, University of St. Andrews, Fife KY16 9ST, United Kingdom

Received: March 22, 2007; In Final Form: May 11, 2007

Aqueous suspensions of paramagnetic lanthanide oxide nanoparticles have been studied by NMR relaxometry. The observed R_2^* relaxivities are explained by the static dephasing regime (SDR) theory. The corresponding R_2 relaxivities are considerably smaller and are strongly dependent on the interval between the two refocusing pulses. The experimental data are rationalized by assuming the value of the diffusion correlation time, τ_D, to be very long in a layer with adsorbed xanthan on the particle's surface. In this layer, the refocusing pulses are fully effective and $R_2 \approx 0$. Outside this layer, the diffusion model for weakly magnetized particles was applied. From the fit of the experimental relaxation data with this model, both the particle radii (r_p) and the radii of the spheres, within which the refocusing pulses are fully effective (r_{diff}), were estimated. The values of r_p obtained are in agreement with those determined by dynamic light scattering. Because the value of r_{diff} depends on the external magnetic field B and on the magnetic moment of the lanthanide of interest (μ_{eff}^2), the R_2 relaxivity was found to be proportional to B and to μ_{eff}^2.

1. Introduction

During the last decades, the rapid progress in biochemical research has provided detailed insight into molecular recognition processes. These developments enable the design of contrast agents (CAs) for molecular imaging[1] with medical diagnostic techniques including positron emission tomography (PET), single photon emission computed tomography (SPECT), and magnetic resonance imaging (MRI). MRI has a significantly higher spatial resolution (μm) than radiodiagnostic techniques (mm), but its use as a tool for the investigation of cellular molecular events in normal and pathological processes is hampered by its low sensitivity: a relatively large local concentration of CA is required (about 10^{-5} M) to achieve the desired contrast enhancement.[2,3] Other imaging modalities such as PET, SPECT ($10^{-11}-10^{-12}$ M), and optical fluorescence imaging ($10^{-15}-10^{-17}$ M) are much more adequate in this respect.[4]

A possible approach to overcome the problems related with the low sensitivity of MRI is to apply vectorized CAs, which would bring a high payload of paramagnetic compound to the site of interest. For lanthanide ion based contrast agents, this was realized in various ways and different materials have been proposed including: Gd-loaded apoferritin, which allows the visualization of hepatocytes when the number of Gd-complexes per cell is about 4×10^7,[5] perfluorocarbon nanoparticles, which contain around 94 200 Gd^{3+} ions per particle providing extremely high relaxivity per particle and which have been already successfully used in molecular imaging of angiogenesis.[6−10]

Alternatively, this may be achieved with superparamagnetic (SPM) particles, single domain ferromagnets possessing a very high magnetic moment (around 10^4 μ_B).[11,12] SPM particles have a much smaller effect on the T_1 water proton relaxation time than on the T_2. Their relaxivity can be well described by the quantum mechanical outer-sphere theory. Because of their small size (20−60 nm in diameter), the extreme motional narrowing conditions are satisfied, which state that water diffusion between SPM particles is rapid with respect to the difference in resonance frequencies of the various sites. In this regime the T_2^* relaxation time is predicted to be equal to T_2. When iron−oxide particles are compartmentalized within cells, the internal magnetization of the compartment due to their presence has to be taken into account. In this situation the motional narrowing assumption breaks down, which results in R_2^* ($= 1/T^*_2$) to be larger than R_2. Consequently, R_2^*-weighted MRI images are potentially the most sensitive to the presence of cellularly compartmentalized magnetized particles.[13−15]

Nanozeolites present another approach. Gd^{3+} exchanged zeolite NaY nanoparticles of an average size of 80 nm, contain about 40 000 Gd^{3+} ions per particle. The longitudinal relaxivity r_1 (r_1 is the relaxation rate expressed in s^{-1} mM^{-1} Gd) is limited by the water exchange between the interior of zeolites and the bulk.[16] It was observed that r_2 relaxivity is independent of the pore structure of the zeolite and that it increases with the external field strength.[17] In materials like Ln−AV-9, which have Ln^{3+} ions incorporated in the zeolite framework, direct interaction between Ln^{3+} ions and water molecules is impossible. As a result, they have a very low r_1 relaxivity, but at the same time they have a very strong impact on the T_2 relaxation.[18]

* To whom correspondence should be addressed. E-mail: J.A.Peters@tudelft.nl.
[†] Biocatalysis and Organic Chemistry, Delft University of Technology.
[‡] University of Coimbra.
[§] Physical Chemistry and Molecular Thermodynamics, Delft University of Technology.
[#] University of St. Andrews.

10.1021/jp072288l CCC: $37.00 © 2007 American Chemical Society
Published on Web 06/23/2007

In this paper we present a study on lanthanide oxide (Ln_2O_3) nanoparticles. These particles have a very high density of Ln^{3+} ions, and their magnetic properties are good candidates for R_2-weighted imaging, and therefore, after coating and attachment of targeting vectors, they may have potential as CAs in molecular imaging with MRI.

2. Experimental Section

The lanthanide oxide nanoparticles were purchased from Aldrich and had a diameter of less than 40 nm as determined with XRD by the supplier.

Water proton transverse relaxation times, T_2, were measured at 20, 60 MHz (Mini-spec PC120 and PC160, respectively, spin analyzers obtained from Bruker), 200 MHz (on a Bruker Avance-200 console connected to a 200 MHz cryomagnet), 300 MHz (Varian INOVA spectrometer), 400 MHz (Varian VXR-400 S spectrometer), and 500 MHz (Varian Unity 500 spectrometer) using the Carr−Purcell−Meiboom−Gill pulse sequence (CPMG). The values of T_2^* were evaluated from the linewidths. All experimental values of relaxation rates were corrected for diamagnetic contributions using a solution of 1 wt % of xanthan in water.

The Ln_2O_3 suspensions for relaxometric studies were prepared by mixing the solid particles with doubly distilled water containing 1 wt % of xanthan gum as a surfactant and dispersing them in an ultrasonic bath for 5 min.

The self-diffusion coefficient of the samples was measured on the 200 MHz spectrometer equipped with a variable-temperature high-resolution diffusion probe. A PGMSE pulse sequence was used for the determination of the diffusion constants. The temperature was maintained by water circulation in the gradient coil. The calibration of the gradients was performed on pure H_2O.

High-resolution transmission electron microscopy (HRTEM) was performed on a Jeol JEM-2010 electron microscope operated at 200 kV.

Dynamic light scattering (DLS) was performed with a DLS/SLS/ALV-5000 apparatus using a 35 mW HeNe laser with a wavelength of 633 nm. The intensity autocorrelation function was measured at an angle of 90° and analyzed with the CONTIN method. All samples were placed in an ultrasonic bath and were centrifuged prior to the DLS measurements in order to remove dust and other contaminants.

3. Results and Discussion

The bulk magnetic susceptibility shifts and the R_1, R_2, and R_2^* relaxivities of aqueous suspensions of Ln_2O_3 particles (Ln = Nd, Gd, Er, Dy, Yb) with an average particle size of less than 40 nm (as determined by XRD) were measured. Suspensions of these nanoparticles in pure water were stable for several days, but upon inserting the samples in magnets with a magnetic field strength of more than 7 T, coagulation and precipitation of the particles occurred. In order to avoid this, 1 wt % xanthan gum was added to the water. TEM and HRTEM images of the Dy_2O_3 nanoparticles (see Figure 1) show that these particles, in the dry form, are fiberlike agglomerates consisting of nanosized plates with a size of 5−10 nm. The measured d-spacings from the HRTEM images indicate that these particles are cubic Dy_2O_3 with $a = 1.067$ nm. Unfortunately, it was impossible to perform dynamic light scattering measurements on the suspensions used for the NMR relaxometric study because the particle density and the xanthan concentration were too high. In more dilute suspensions (without xanthan), fractions with particles sizes of about 50−100 nm were observed after ultrasound treatment (see Figure S1 in the Supporting Information). Therefore, we assume that the agglomerates break down into a homogeneous suspension of nanoparticles upon ultrasonic treatment in the presence of xanthan.

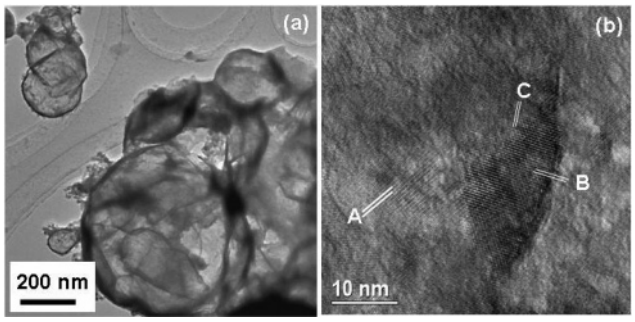

Figure 1. (a) TEM image of dysprosium oxide showing fiberlike morphology and (b) corresponding HRTEM image showing nanoparticles. The marked d-spacings are measured as (A) 0.52, (B) 0.42, and (C) 0.31 nm, which can be indexed onto the cubic unit cell of Dy_2O_3 with $a = 1.07$ nm as (200), (−121), and (311), respectively.

TABLE 1: Comparison of Δ_{BMS} of Suspensions[a] of Ln_2O_3 in a Solution of 1 wt % of Xanthan in Water and Homogeneous Solutions Obtained after Addition of HCl at 7 T and 25 °C

	Δ_{BMS}/ppm suspensions	Δ_{BMS}/ppm homogeneous solutions[b]
Gd	0.37 ± 0.03	0.36 ± 0.03
Er	0.48 ± 0.04	0.47 ± 0.04
Dy	0.45 ± 0.04	0.49 ± 0.05

[a] Containing 1.3−1.6 mmol Ln_2O_3/L water. [b] Obtained by adding HCl to suspensions; Δ_{BMS} was corrected for changes in volume.

3.1. Bulk Magnetic Susceptibility Shifts. These shifts (Δ_{BMS}) are related to the global magnetization (M) of the lanthanide oxide particles in suspension via eq 1.[19] In eq 1, B

$$\Delta_{BMS} = s\frac{M}{B}10^6 \tag{1}$$

is the magnetic field strength and s is a shape factor. The latter is $^1/_3$ in the present case, where the sample tube was parallel to the magnetic field during the measurement. Since magnetic coupling is negligible for Ln(III) compounds at room temperature,[18] M can be calculated with eq 2. In eq 2, N is the number

$$M = Nn\mu_0\mu_C \tag{2}$$

of the particles per m^3, n is the number of Ln^{3+} ions per particle, μ_0 is the vacuum magnetic permeability, and μ_C is the Curie moment. The latter is given by eq 3, where μ_B is the Bohr magneton, g is the Landé g-factor, J is the quantum number of the total spin, k is the Boltzmann constant, and T is the absolute temperature.

$$\mu_C = \frac{\mu_{eff}{}^2 B}{3kT}, \quad \text{where } \mu_{eff} = g\mu_B\sqrt{J(J+1)} \tag{3}$$

The values of Δ_{BMS} of the suspensions of nanoparticles of three lanthanides oxides were measured at $B = 7$ T and compared with Δ_{BMS} of corresponding homogeneous solutions prepared directly from the suspensions concerned by adding HCl. The data (see Table 1) show that there is no difference between the suspensions and the corresponding homogeneous solutions. It may be concluded that the global magnetizations of these systems are the same, confirming that magnetic coupling is negligible under the conditions applied.

TABLE 2: Parameters Obtained from Analysis of R_2 and R_2^* Values of Aqueous Suspensions of Lanthanide Oxides at $B = 7$ T and $T = 25$ °C[a]

	$\Delta\omega(r_p)\ 10^6$ [1/s][b]	$\Delta\omega(r_p)_{max}\ 10^6$ [1/s][c]	$\tau_D(r_{diff})\ 10^{-4}$ [s][b]	r_p/r_{diff}[b]	r_p [nm][d]	R_2^0 [1/s][b]	$R^*_{2,exp}$ [s^{-1}][e]
Nd_2O_3	0.539 ± 0.002	1.928 ± 0.002	6.6 ± 0.7	0.110 ± 0.004	123 ± 12	1.7 ± 0.1	32 ± 3
Gd_2O_3	3.838 ± 0.003	8.525 ± 0.003	17.4 ± 1.1	0.036 ± 0.001	65 ± 6	9.9 ± 0.2	237 ± 24
Dy_2O_3	4.818 ± 0.027	13.776 ± 0.027	2.8 ± 0.5	0.069 ± 0.004	50 ± 5	21.8 ± 1.6	300 ± 33
Er_2O_3	4.180 ± 0.006	15.569 ± 0.006	5.4 ± 0.5	0.049 ± 0.001	49 ± 5	14.3 ± 0.3	238 ± 25
Yb_2O_3	1.333 ± 0.004	3.302 ± 0.004	4.1 ± 0.6	0.084 ± 0.004	74 ± 7	2.6 ± 0.2	68 ± 6

[a] 1 mmol Ln^{3+}/L water containing 1 wt % xanthan. [b] From fitting of experimental data with eqs 4 and 12. [c] Calculated with eqs 5 and 9. [d] Calculated from the best-fit values of $\tau_D(r_{diff})$, r_p/r_{diff}, and the experimentally determined value of D_0. [e] As evaluated from the experimental linewidths.

TABLE 3: Parameters Obtained from Analysis of R_2 and R_2^* Values of an Aqueous Suspension of Dy_2O_3 at $T = 25$ °C[a]

B [T]	$\Delta\omega(r_p)\ 10^6$ [1/s][b]	$\tau_D(r_{diff})\ 10^{-4}$ [s][b]	r_p/r_{diff}[b]	r_p [nm][c]	R_2^0 [1/s][b]	$R^*_{2,exp}$ [s^{-1}][e]
0.47	0.4[d]	35.3 ± 2.4	0.071 ± 0.005	184 ± 18	1.1 ± 0.02	
1.4	1.1[d]	7.0 ± 1.02	0.077 ± 0.005	89 ± 9	3.2 ± 0.2	
4.7	4.7 ± 0.013	7.3 ± 0.99	0.046 ± 0.002	54 ± 5	18.1 ± 0.7	290 ± 80
7.0	4.8 ± 0.027	2.8 ± 0.47	0.069 ± 0.004	50 ± 5	21.8 ± 1.6	300 ± 33
9.4	7.2 ± 0.033	9.4 ± 1.29	0.044 ± 0.002	58 ± 6	37.1 ± 1.8	454 ± 50
11.7	9.6 ± 0.097	2.0 ± 0.49	0.066 ± 0.005	41 ± 4	40.9 ± 5.6	593 ± 60

[a] 1 mmol Dy^{3+}/L water containing 1 wt % xanthan. [b] From fitting of experimental data with eqs 4 and 12. [c] Calculated from the best-fit values of $\tau_D(r_{diff})$, r_p/r_{diff}, and the experimentally determined value D_0. [d] Extrapolated from the values of the best-fit of data measured at 4.7, 7.0, 9.4, and 11.4 T. This parameter was fixed during the fitting. [e] As evaluated from the experimental linewidths.

3.2. Relaxation Rates (R_1, R_2^*, and R_2). The Ln_2O_3 nanoparticles have almost no effect on longitudinal relaxation times (T_1) of the ^{1}H water resonance; the T_1 values observed in a suspension containing 1 mM Ln were 2−3 s, except for the suspension with Gd_2O_3, which had a T_1 value of 0.6 s (see Supporting Information, Table S1).

By contrast, the effects on the transversal relaxation rates were substantial. The linewidths of the ^{1}H water resonance of suspensions of the paramagnetic lanthanide oxides were large in comparison to those of the diamagnetic La_2O_3 suspension (20 Hz), which after subtraction of the line width for a xanthan solution in pure water gives a linewidth of 8 Hz. From the linewidths of samples measured, values of R_2^* were evaluated (see Tables 2 and 3).

The line-broadenings can be ascribed to susceptibility induced R_2 enhancements as a result of the diffusion of water molecules in the field inhomogeneities created by the magnetized particles. The magnetic field changes in space leading to differences in the Larmor frequencies of the protons. The proton Larmor frequency at a particular location is given by the relation $\omega = \gamma B_{loc}$, where ω is the proton Larmor frequency (in rad s^{-1}) and B_{loc} is the local strength of the magnetic field. The diffusion of water protons between different magnetic environments reduces their phase coherence and, consequently, causes effective T_2-shortening.

The transverse relaxation rates (R_2) were determined by means of the Carr−Purcell−Meiboom−Gill pulse sequence (CPMG). These measurements all showed a perfect monoexponential decay, which is characteristic for magnetic compounds enhancing the water proton relaxivity by diffusion.[20] The CPMG measurements were performed as a function of the time distance between two consecutive refocusing pulses (τ_{CP}) in the train of 180° pulses applied.[21−23] Figures 2 and 3 show the dependence of R_2 on τ_{CP} for various lanthanide oxides at a single magnetic field and for Dy_2O_3 at different magnetic fields, respectively. The values of R_2 obtained are much smaller than the corresponding R_2^* values and appeared to be strongly dependent on τ_{CP}. This behavior is characteristic for a system in the static dephasing regime (SDR), where the condition $\tau_D > \Delta\omega(r_p)^{-1}$ holds ($\tau_D = r_p^2/D$, where r_p is the radius of the particle, D is the water diffusion coefficient, and $\Delta\omega(r_p)$ is the Larmor frequency shift at the particle's surface). Under this condition, the relaxation rate R_2^* can be ascribed to the dephasing of *motionless* magnetic moments in a nonuniform field created by randomly distributed magnetic particles.[24−29] The value of R_2^* is then given by eq 4:

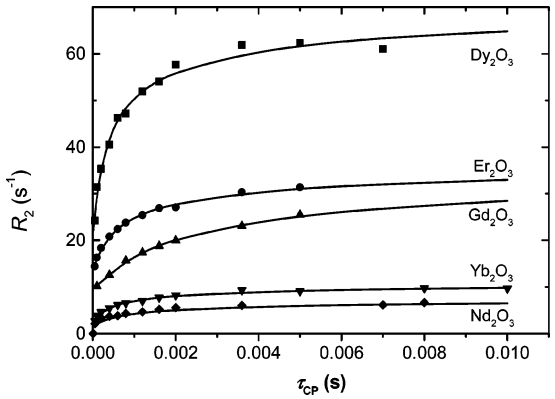

Figure 2. Dependence of R_2 on τ_{CP} for different lanthanide oxide nanoparticles at 7 T and 25 °C; the curves are fits of the experimental data to eq 4 and 12 (for more details see text); the suspensions always contained 1 mmol Ln^{3+}/L water with 1 wt % xanthan.

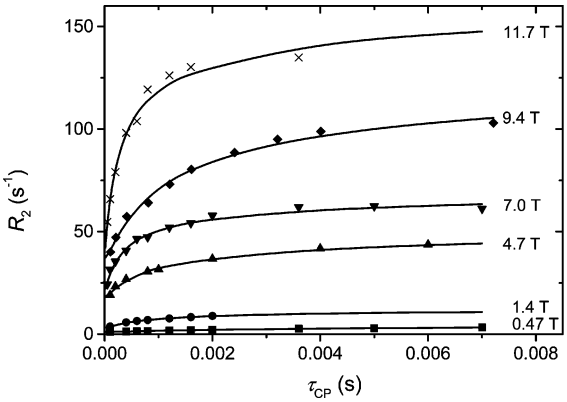

Figure 3. Dependence of R_2 on τ_{CP} measured in different external magnetic fields at 25 °C; the curves are fits of the experimental data to eq 4 and 12 (for more details see the text); the suspensions always contained 1 mmol Dy^{3+}/L water with 1 wt % xanthan.

$$R_2^* = \frac{1}{T_2^*} = R_2^0 + 2\pi\sqrt{3} f \Delta\omega(r_p)/9 \quad (4)$$

Here, $f = vN$ is the volume fraction occupied by the particles (v is the volume of a single particle and N is the number of particles per m^3) and R_2^0 is the contribution due to other relaxation mechanisms, such as the diamagnetic relaxation and a contribution as the result of chemical exchange of protons between the surface of the particles and the bulk water protons. Equation 4 was developed for spherical particles. The error introduced by this simplification may be neglected, since the magnetic field created by any particle is sensitive to its shape only in close proximity of the particle. For low concentrations of lanthanide oxide particles (f was always $\sim 10^{-5}$), one can assume that the majority of water protons experience field gradients created by approximately spherically shaped particulates. Since both f and $\Delta\omega(r_p)$ are not dependent on the particle radius r_p, the values of R_2^* are independent of the particle size as well.

The angular frequency shift at the surface of the particle, $\Delta\omega(r_p)$, is related to the magnetization of a single particle, M_p, and will be strongly dependent on the shape of the particles. Its maximal value is that of a spherical particle, for which the value of this parameter can be estimated by eq 5, where, γ is the proton gyromagnetic ratio.[30] For paramagnetic particles it

$$\Delta\omega(r_p) = \gamma M_p/3 \quad (5)$$

can be assumed that, upon placement in a magnetic field, a macroscopic magnetic moment is forming in each single particle, which is parallel to the external magnetic field. The magnitude of this magnetic moment is given by eqs 6−8.

$$M_p = \frac{n}{v}\mu_0 g \mu_B J B_J(x) \quad (6)$$

$$x = \frac{gJ\mu_B B}{kT} \quad (7)$$

$$B_J(x) = \frac{2J+1}{2J} ctgh\left(\frac{(2J+1)x}{2J}\right) - \frac{1}{2J} ctgh\left(\frac{x}{2J}\right) \quad (8)$$

The latter is the Brillouin function and μ_0 and J are the vacuum magnetic permeability and the quantum number of the total spin, respectively. For the temperature at which the samples were measured, $x \ll 1$, and then eq 6 can be simplified to

$$M_p = \frac{n}{v}\mu_0 \mu_C \quad (9)$$

M_p was obtained using the particle volumes (v) and n values evaluated from their size (as determined from DLS) and the known density of the Ln_2O_3 in question. The magnitude of $\Delta\omega(r_p)$ as determined by eqs 5 and 9 will give an upper limit of this parameter; nonspherical particles and agglomerates of particles will have lower values. Values for $\Delta\omega(r_p)_{max}$ as calculated from eqs 5 and 9 are included in Table 2.

The dependence of R_2 on τ_{CP} for strongly magnetized particles ($\tau_{CP}\Delta\omega(r_p) > 1$) in the static dephasing regime has been analyzed by Gillis et al. and explained by the partial refocusing model.[29]

The behavior of R_2 as a function of τ_{CP} relies on a spatial division between an inner region ($\Delta\omega(r) > \tau_{CP}^{-1}$) according to this model, where the refocusing pulses are not effective due to the extremely high gradients close to the particles surface and an outer one ($\Delta\omega(r) < \tau_{CP}^{-1}$), where the refocusing pulses are partially effective due to effects of weak field inhomogeneities (far away from the particles surface). The radius of the sphere that forms the border between the two regions (r_{SDR}) depends on τ_{CP}. The overall relaxivity is considered as being the weighted sum of two components: a fast one coming from the inner and a slow one from the outer region. For relatively small τ_{CP}, the relaxivity is assumed to rest exclusively on the contribution from the outer region. The model predicts that upon the increase of τ_{CP}, the contribution from the inner region becomes increasingly important (the fast component in the signal starts to dominate), resulting in the progressive increase of the R_2 relaxivity until the maximal possible value, characterized by R_2^* (R_2 [$\tau_{CP} \rightarrow \infty$] = R_2^*). Surprisingly, attempts to fit the present experimental data with the partial refocusing model failed (see Supporting Information); a leveling off of the curves of R_2 as a function of τ_{CP} at R_2^* could not be obtained, the best-fit values of $\Delta\omega(r)$ were significantly smaller than those calculated from particle sizes as determined by DLS and eq 5 and 9, and the best-fit values of r_p were much larger than those determined by DLS, and they appeared to be strongly dependent on the magnetic field strength, which is unlikely.

We attribute this behavior to the xanthan gum that we applied as an emulsifier. It is known that it may adsorb in a thick layer on oxide surfaces.[31] Therefore, the diffusion of water molecules near the surface may be relatively slow due to formation of hydrogen bonds with the adsorbed xanthan chains. If in this layer the condition $\tau_D \gg \Delta\omega(r_p)^{-1}$ holds, the diffusion correlation time is not effective when refocusing pulses are applied and, consequently, the phase incoherence of the water protons is fully refocused resulting in an R_2 value approaching zero.[32]

Let us consider this situation when no refocusing pulses are applied. Upon increase of the distance from the particle's center, r ($r > r_p$), protons will feel the field inhomogeneities caused by the magnetization of the particle in a decreasing extent. In the xanthan layer, we suppose that the condition $\tau_D(r) > \Delta\omega(r)^{-1}$ holds and then the effect of diffusion is negligible (SDR). Near the outside of this layer, the condition $\tau_D(r) < \Delta\omega(r)^{-1}$ will be fulfilled at some distance from the particle surface. Because, there, diffusion introduces unrecoverable losses of the phase coherence, refocusing pulses are no longer fully efficient in this part of the sample, resulting in nonzero R_2 relaxivity in the CPMG experiment. The radius of a sphere defining the boundary between the two regions (r_{diff}) can be roughly estimated by assuming that this boundary is defined by $\tau_D(r) = \Delta\omega(r)^{-1}$ (see eq 10). Then this radius is given by eq 11.

$$\tau_D(r_p)\left(\frac{r_{diff}}{r_p}\right)^2\left(\frac{D}{D_0}\right) = \tau_D(r_{diff}) = \frac{1}{\Delta\omega(r_{diff})} = \frac{1}{\Delta\omega(r_p)}\left(\frac{r_{diff}}{r_p}\right)^3 \quad (10)$$

$$r_{diff} = \frac{\Delta\omega(r_p) r_p^3}{D_0} \quad (11)$$

Here, D_0 is assumed to be unrestricted and corresponds to the majority of water protons at some distance from the surface of the particle.

For the refocusing pulses to be efficient, at the same time, the condition $\tau_{CP} \ll \tau_D$ must be fulfilled.[33,34] Taking into account that the protons in the layer between the spheres with radii of r_p and r_{diff} do not contribute to the relaxivity, we consider the

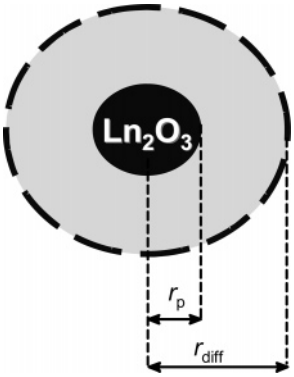

Figure 4. Schematic representation of the model applied to analyze the transverse relaxation behavior of aqueous suspensions of paramagnetic lanthanide oxides. The shaded area around the lanthanide oxide particle represents the layer, which does not contribute to the relaxivity, $R_2 = 0$.

system as consisting of magnetic particulates of radius r_{diff} rather than r_p (see Figure 4). Consequently, the system is characterized by $\tau_D(r_{diff})$ and $\Delta\omega(r_{diff})$. In this situation $\tau_D(r_{diff})$ can be relatively high, since $r_{diff} > r_p$. The field gradient caused by the strongly magnetized particles is rapidly decreasing upon increasing the distance to the particle and, therefore, we expect that the field inhomogeneities are weak in character outside the sphere with radius r_{diff}. Then, the theory of Jensen and Chandra for weak field inhomogeneities can be applied.[35] Assuming a Gaussian shape of the field correlation function, these authors derived the following equations (for irregular objects and unrestricted diffusion):

$$R_2 = R_2^0 + {}^1/_2\Delta\omega(r_{diff})^2 f(r_{diff})\tau_D(r_{diff})F(x) \qquad (12)$$

where

$$F(x) = \frac{1}{\sqrt{\pi}}\int_0^\infty dy\,\frac{e^{-y}}{\sqrt{y}}\left[1 - \frac{1}{xy}\tanh(xy)\right] \quad \text{and } x = \frac{4\tau_{CP}}{\tau_D(r_{diff})}$$

The values of $\Delta\omega(r_{diff})$, $\tau_D(r_{diff})$, and $f(r_{diff})$ can be expressed as follows:

$$\Delta\omega(r_{diff}) = \Delta\omega(r_p)\left(\frac{r_p}{r_{diff}}\right)^3 \qquad (13)$$

$$\tau_D(r_{diff}) = \tau_D(r_p)\left(\frac{r_{diff}}{r_p}\right)^2\left(\frac{D}{D_0}\right) \qquad (14)$$

$$f(r_{diff}) = f(r_p)\left(\frac{r_{diff}}{r_p}\right)^3 \qquad (15)$$

For $x \ll 1$, $F(x) = x^2/4$, and for $x \gg 1$, $F(x) = 1$. Thus,

$$R_2 = R_2^0 + \frac{1}{2}\Delta\omega(r_{diff})^2 f(r_{diff})\frac{{\tau_{CP}}^2}{\tau_D(r_{diff})} \quad \text{for } \tau_{CP} \ll \tau_D(r_{diff}) \qquad (16)$$

and

$$R_2 = R_2^0 + \frac{1}{2}\Delta\omega(r_{diff})^2 f(r_{diff})\tau_D(r_{diff}) \quad \text{for } \tau_{CP} \gg \tau_D(r_{diff}) \qquad (17)$$

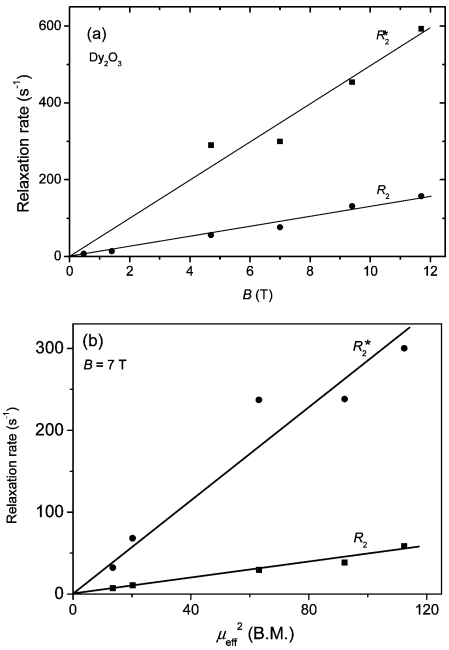

Figure 5. (a) The dependence of R_2 (slope 13.0 s^{-1} T^{-1}; $r = 0.992$) and R_2^* (slope 49.5 s^{-1} T^{-1}; $r = 0.985$) of an aqueous suspension of Dy_2O_3 on the external magnetic field B. (b) The dependence of R_2 (slope 0.48 s^{-1} μ_B^{-2}; $r = 0.989$) and R_2^* (slope 2.8 s^{-1} μ_B^{-2}; $r = 0.972$) of an aqueous suspension of lanthanide oxide nanoparticles on μ_{eff}^2. All R_2 values presented in the graphs were calculated for $\tau_{CP} = 1$ s, and the concentrations of the samples were about 0.5 mM.

The experimental data (R_2 and R_2^*) were fitted simultaneously with eqs 4 and 12 using $\Delta\omega(r_p)$, $\tau_D(r_{diff})$, r_p/r_{diff}, and R_2^0 as adjustable parameters. An excellent agreement between the experimental and calculated values was achieved. The best-fit parameters are listed in Tables 2 and 3, whereas the calculated curves are displayed in Figures 2 and 3. The values $\tau_D(r_{diff})$ are all in the milliseconds range, which is in agreement with the observed dependence of R_2 on τ_{CP}. The smallest τ_{CP} value applied was 5×10^{-5} s, so it is evident that the condition $\tau_{CP} \ll \tau_D(r_{diff})$ is met. When τ_{CP} approaches $\tau_D(r_{diff})$, the system reaches the motional narrowing regime, where refocusing pulses are no longer efficient and, consequently, the curves of R_2 versus τ_{CP} levels off at $\tau_{CP} > \tau_D(r_{diff})$. The obtained values of $\tau_D(r_{diff})$ (see Tables 2 and 3) correspond very well with the values of τ_{CP}, where the curves start to saturate (see Figures 2 and 3). For example, the longest $\tau_D(r_{diff})$ was obtained for Gd_2O_3, and this is reflected in a relatively low initial slope of the corresponding curve.

r_p can be determined by knowing $\tau_D(r_{diff})$, r_p/r_{diff}, and the diffusion coefficient D_0. D_0 was measured by the pulsed gradient multiple spin echo pulse sequence, PGMSE, and was found to be 1.9×10^{-9} m^2 s^{-1}. The resulting values of r_p, gathered in Tables 2 and 3, are in good agreement with the results of the DLS analyses. The evaluated particle radii show a decreasing trend upon increase of the magnetic field (see Table 3), which probably is due to the crudeness of the model applied.

The best-fit values of R_2^0 are considerable (see Tables 2 and 3). The diamagnetic contribution to R_2^0 was estimated from measurements on suspensions of La_2O_3 nanoparticles and appeared to be less than 1. Possibly R_2^0 includes an additional contribution from the chemical exchange between protons on the particles surface and bulk water. However, R_2^0 depends linearly on both B and μ_{eff}^2 while for chemical exchange a quadratic dependence would be expected. Therefore, it cannot

be excluded that the values R_2^0 also include a contribution that corrects for the simplifications in the model.

The values of R_2^* and the saturation values of R_2 are both proportional to the external magnetic field B as well as to μ_{eff}^2 (see Figure 5). For R_2^*, this is in agreement with eq 4, which shows a linear relationship between R_2^* and $\Delta\omega(r_p)$, which is proportional to B and μ_{eff}^2.

Substitution of eqs 13−15, which relate $\Delta\omega(r_{diff})$, $\tau_D(r_{diff})$, and $f(r_{diff})$ to $\Delta\omega(r_p)$, $\tau_D(r_p)$, and $f(r_p)$, respectively, for spherical particles, in eq 17, gives eq 18. Taking into consideration eq

$$R_2 = R_2^0 + \frac{1}{2}\Delta\omega(r_p)^2 f(r_p)\tau_D(r_p)\left(\frac{r_p}{r_{diff}}\right)\left(\frac{D}{D_0}\right) \qquad (18)$$

11, which gives a rough estimate of r_{diff}, it can be concluded that $R_2 \approx \Delta\omega(r_p)f$. Since $\Delta\omega(r_p)$ is proportional to B and μ_{eff}^2, and the results of the fittings described above show that the same holds for R_2^0, it can be concluded that R_2 is proportional to B and μ_{eff}^2 as well, which is in agreement with the results presented in Figure 5.

Equation 18 also demonstrates that R_2 is proportional to the diffusion constant in close proximity of the particle's surface (D) relative to that of bulk water (D_0). This is in agreement with the expected increase of the importance of the relaxation process due to diffusion of water protons in local magnetic field gradients upon increase of D and thus with increasing distance to the surface of the particle, since more efficient diffusion leads to less recovery of phase coherence by the refocusing pulses.[21]

4. Conclusions

Paramagnetic Ln_2O_3 particles behave as strongly magnetized particles and, as a result of the magnetic field inhomogeneities, they induce large ^{1}H transverse relaxation rate enhancements in aqueous suspensions. Although these particles show paramagnetic behavior,[36−39] the magnitude of this effect is comparable with the effect caused by SPM particles.[40−43] For instance, AMI25 dextran coated magnetite particles have $M_p = 8.2 \times 10^{-2}$ T,[25] while for Dy_2O_3 M_p can be calculated to be 16.9×10^{-2} T at $B = 7$ T. However, the field dependence of the global magnetizations of the particle suspensions differs significantly. At a weak external magnetic field ($B < 1$ T), the values of M for SPMs are about 5 orders of magnitude larger than those for paramagnetic particles and get saturated already in a magnetic field of about 1 T.

Both R_2^* and R_2 values of Ln_2O_3 nanoparticles are linearly dependent on the strength of the external magnetic field, B. At present, there is a tendency to perform MRI exams at higher magnetic fields. Lanthanide oxides have favorable relaxivity properties for these higher fields.

The results described suggest that an R_2-silent layer exists around the particles, which may be attributed to adsorption of xanthan, which was applied as an emulsifier. It may be expected that much higher R_2 relaxivities will be obtained when the particles are surface treated with a thinner layer of coating. Optimally, paramagnetic lanthanide oxide nanoparticles will behave as strongly magnitized particles, and then the highest relaxivities should be expected for particle radii which are such that the system is on the border between the regions where the outer sphere and the SDR theories are valid.[29]

For the practical application as a MRI contrast agent, the lanthanide oxide particles should be protected against leaching of highly toxic free Ln^{3+} ions by an appropriate coating, for example, with a dextran of a polysiloxane shell.[44] Attachment of additional functions, such as PEG groups, may improve the biodistribution and, furthermore, these particles can, if conjugated to the appropriate targeting vector, deliver a high payload of Ln^{3+} at the site of interest. The results of the present study may be helpful for the design of particles with optimal size and thickness of surface coatings.

Recently, McDonald and Watkin have shown that Gd_2O_3 nanoparticles become superparamagnetic upon coating.[45,46] It may be expected that the oxides of other paramagnetic lanthanides will also become superparamagnetic upon coating. Further studies to investigate this are in progress.

Acknowledgment. We thank Prof. R. N. Muller, Prof. P. Gillis, and Dr. A. Roch of the University of Mons-Hainaut, Belgium, for their kind help in measuring relaxivities at low magnetic fields and for helpful discussions. Thanks are due to the EU for financial support via a Marie Curie training site host fellowship (Grant MEST-CT-2004-7442), to the Foundation of Science and Technology (FCT), Portugal, (Project POCTI/QUI/47005/2002), and to FEDER. This work was done in the frame of COST Action D38 "Metal-Based Systems for Molecular Imaging Applications" and the EU Network of Excellence European Molecular Imaging Laboratory" (EMIL, Grant LSCH-2004-503569).

Supporting Information Available: DLS pictures of lanthanide oxide particles, T_1 values of ^{1}H water resonances in suspensions of lanthanide oxides, and fitting of the experimental R_2 data using the partial refocusing model. This material is available free of charge via the Internet at http://pubs.acs.org.

References and Notes

(1) Weissleder, R.; Mahmood, U. *Radiology* **2001**, *219*, 316−333.
(2) Ahrens, E. T.; Rothbächer, U.; Jacobs, R. E.; Fraser, S. E. *Proc. Natl. Acad. Sci. U.S.A.* **1998**, *95*, 8443−8448.
(3) Mills, P. H.; Ahrens, E. T. *Magn. Reson. Med.* **2007**, *57*, 442−447.
(4) Weissleder, R. *Radiology* **1999**, *212*, 609−614.
(5) Aime, S.; Cabella, C.; Colombatto, S.; Crich, S. G.; Gianolio, E.; Maggioni, F. *J. Magn. Reson. Imaging* **2002**, *16*, 394−406.
(6) Morawski, A. M.; Winter, P. M.; Crowder, K. C.; Caruthers, S. D.; Fuhrhop, R. W.; Scott, R. W.; Robertson, J. D.; Abendschein, D. R.; Lanza, G. M.; Wickline, S. A. *Magn. Reson. Med.* **2004**, *51*, 480−486.
(7) Winter, P.; Athey, P.; Kiefer, G.; Gulyas, G.; Frank, K.; Fuhrhop, R.; Robertson, D.; Wickline, S. A.; Lanza, G. *J Magn. Magn. Mater.* **2005**, *293*, 540−545.
(8) Winter, P. M.; Caruthers, S. D.; Kassner, A.; Harris, T. D.; Chinen, L. K.; Allen, J. S.; Lacy, E. K.; Zhang, H.; Robertson, J. D.; Wickline, S. A.; Lanza, G. M. *Cancer Res.* **2003**, *63*, 5838−5843.
(9) Winter, P. M.; Morawski, A. M.; Caruthers, S. D.; Fuhrhop, R. W.; Zhang, H.; Wiliams, T. A.; Allen, J. S.; Lacy, E. K.; Robertson, J. D.; Lanza, G. M.; Wickline, S. A. *Circulation* **2003**, *108*, 2270−2274.
(10) Flacke, S.; Fisher, S.; Scott, M. J.; Fuhrhop, R.; Allen, J. S.; McLean, M.; Winter, P.; Sicard, G. A.; Gaffney, P. J.; Wickline, S. A.; Lanza, G. M. *Circulation* **2001**, *104*, 1280−1285.
(11) Muller, R. N.; Roch, A.; Colet, J.-M.; Ouakssim, A.; Gillis, P. In *The Chemistry of Contrast Agents in Medical Magnetic Resonance Imaging*; Merbach, A. É.; Tóth, É., Eds.; John Wiley and Sons: Chichester, U.K., 2001; Chapter 10.
(12) Muller, R. N.; Vander Elst, L.; Roch, A.; Peters, J. A.; Csajbók, É.; Gillis. P.; Gossuin, Y. *Adv. Inorg. Chem.* **2005**, *57*, 239−292.
(13) Bowen, C. V.; Zhang, X.; Saab, G.; Gareau, P. J.; Rutt, B. K. *Magn. Reson. Med.* **2002**, *48*, 52−61.
(14) Foster-Gareau, P.; Heyn, C.; Alejski, A.; Rutt, B. K. *Magn. Reson. Med*. **2003**, *49*, 968−971.
(15) Heyn, C.; Bowen, C. V.; Rutt, B. K.; Foster, P. J. *Magn. Reson. Med*. **2005**, *53*, 312−320.
(16) Platas-Iglesias, C.; Vander Elst, L.; Zhou, W.; Muller, R. N.; Geraldes, C. F. G. C.; Maschmeyer, T.; Peters, J. A. *Chem.—Eur. J*. **2002**, *8*, 22.
(17) Csajbók, É.; Bányai, I.; Vander Elst, L.; Muller, R. N.; Zhou, W.; Peters, J. A. *Chem.—Eur. J.* **2005**, *11*, 4799−4807.
(18) Pereira, G. A.; Ananias, D.; Rocha, J.; Amaral, V. S.; Muller, R. N.; Vander Elst, L.; Tóth, É.; Peters, J. A.; Geraldes, C. F. G. C. *J. Mater. Chem.* **2005**, *15*, 3832−3837.

(19) Chu, S. C.-K.; Xu, Y.; Balschi, J. A.; Springer, C. S., Jr. *Magn. Reson. Med.* **1990**, *13*, 239−262.
(20) Gossuin Y.; Roch A.; Muller R. N.; Gillis, P. *J. Magn. Reson.* **2002**, *158*, 36−42.
(21) Hardy, P. A.; Henkelman, R. M. *Magn. Reson. Imaging* **1989**, *7*, 265−275.
(22) Hardy, P. A.; Henkelman, R. M. *Magn. Reson. Med.* **1991**, *17*, 348−356.
(23) Jensen, J. H.; Chandra, R. *Mag. Reson. Med.* **2000**, *43*, 226−236.
(24) Brown, R. J. S. *Phys. Rev.* **1961**, *121*, 1379−1382.
(25) Muller, R. N.; Gillis, P.; Moiny, F.; Roch, A. *Magn. Reson. Med.* **1991**, *22*, 178−182.
(26) Weisskoff, R. M.; Zuo, C. S.; Boxerman, J. L.; Rosen, B. R. *Magn. Reson. Med*. **1994**, *31*, 601−610.
(27) Yablonskiy, D. A.; Haacke, E. M. *Magn. Reson. Med.* **1994**, *32*, 749−763.
(28) Koenig S. H. *Invest. Radiol*. **1998**, *11*, 822−827.
(29) Gillis, P.; Moiny, F.; Brooks, R. A. *Magn. Reson. Med.* **2002**, *47*, 257−263.
(30) Roch, A.; Gossuin, Y.; Muller, R. N.; Gillis, P. *J. Magn. Magn. Mater*. **2005**, *293*, 532−539.
(31) Li, H.-Y. *Chem. Res. Chin. Univ.* **2004**, *20*, 501−503.
(32) Yung K.-T. *Magn. Reson. Imaging* **2003**, *21*, 451−463.
(33) Brooks, R. A.; Moiny, F.; Gillis, P. *Magn. Reson. Med.* **2001**, *45*, 1014−1020.
(34) Gossuin, Y.; Roch, A.; Muller, R. N.; Gillis, P. *Magn. Reson. Med*. **2000**, *43*, 237−243.
(35) Jensen, J. H.; Chandra, R. *Magn. Reson. Med.* **2000**, *44*, 144−156.
(36) Nelson, J. A.; Bennett, L. H.; Wagner, M. J. *J. Am. Chem. Soc*. **2002**, *124*, 2979.
(37) Nelson, J. A.; Bennett, L. H.; Wagner, M. J. *J. Mater. Chem*. **2003**, *13*, 857−860.
(38) Rowley, A. T.; Parkin, I. R. *Inorg. Chim. Acta* **1993**, *211*, 77−80.
(39) Roberts, D.; Zhu, W. L.; Frommen, C. M.; Rosenzweig, Z. *J. Appl. Phys.* **2000**, *87*, 6208−6210.
(40) Pankhurst, Q. A.; Connolly, J.; Jones, S. K.; Dobson, J. *J. Phys. D: Appl. Phys*. **2003**, *36*, R167−R181.
(41) Bulte, J. W. M.; Brooks, R. A.; Moskowitz, B. M.; Bryant, L. H., Jr.; Frank, J. A. *Magn. Reson. Med*. **1999**, *42*, 379−384.
(42) Brooks, R. A.; Vymazal, J.; Goldfarb, R. B.; Bulte, J. W. M.; Aisen, P. *Magn. Reson. Med*. **1998**, *40*, 227−235.
(43) Mornet, S.; Vasseur, S.; Grasset, F.; Dugnet, E. *J. Mater. Chem.* **2004**, *14*, 2161−2175.
(44) Bridot, J.-L.; Faure, A.-C.; Laurent, S.; Rivière, C.; Billotey, C.; Hiba, B.; Janier, M.; Josserand, V.; Coll, J.-L.; Vander Elst, L.; Muller, R.; Roux, S.; Perriat, P.; Tillement, O. *J. Am. Chem. Soc.* **2007**, *129*, 5076−5084.
(45) McDonald, M. A.; Watkin, K. L. *Invest. Radiol.* **2003**, *38*, 305−310.
(46) McDonald, M. A.; Watkin, K. L. *Acad. Radiol.* **2006**, *13*, 421−427.